

The analysis of fluorescence microscopy images for FRET detection

Ela Claridge¹, Dale J. Powner² and Michael J.O. Wakelam²

¹School of Computer Science, The University of Birmingham B15 2TT, U.K.

²Institute for Cancer Studies, The University of Birmingham, Birmingham B15 2TT, U.K.

Abstract— This paper describes a new method of analysis of fluorescence images containing a mixture of fluorophores. Parametric maps showing the relative quantity and distribution of each individual fluorophore are generated using a predictive model of image formation. Error analysis applied to the model supplies objective criteria for choosing the optimal filters for image acquisition in the regions in the spectra where error is lowest. The method has been successfully applied to the detection of Fluorescence Resonance Energy Transfer (FRET) which provides evidence of interaction between proteins in a cell. The study of protein-protein interactions is of crucial importance in basic biomedical sciences.

I. INTRODUCTION

Individual cells from living organisms can be specifically stimulated by their extracellular environment to perform a defined task, for example a hormone from the blood supply may stimulate cell growth. This requires the transduction of the extracellular stimulant into an intracellular signal. Intracellularly, the transduction of such a signal can be mediated through consecutive modular interaction between two or more proteins. It is probable that the pathology of many diseases results from complete loss or aberrant interactions between such proteins. Although the homogeneous purification of specific proteins facilitates the in vitro characterisation of an interaction, these studies provide no information with regards to the spatial and temporal regulation of interactions within a living cell; information that is likely to be essential to enable future therapeutic interventions. With the aid of standard optical microscopy it is possible to see whether two proteins co-localise (i.e. they are close one to another in the cell), but not whether they interact. To achieve this, the proteins of interest are each tagged with a different coloured fluorescent molecule (fluorophore), for example red and green. Each of the fluorophores is individually stimulated and images of the resulting fluorescence are taken through the matched filters (e.g. red and green). In the registered images yellow hues indicate the locations where both the red and the green fluorophores co-localise. As well as not giving any indication as to whether or not these proteins interact, the reliability of this analysis is sometimes questioned because registration errors or accidental overlap in depth can generate false positives. In Fluorescence

Resonance Energy Transfer imaging (FRET) the proteins of interest are tagged with specially matched fluorophores. One of them will fluoresce only if it is at a Förster distance (1-10 nm) from the other, which is likely to occur only if the two tagged proteins interact. The occurrence of FRET is taken to provide much firmer evidence of interaction, but the FRET induced fluorescence is much weaker than the primary fluorescence and hence difficult to detect reliably.

This paper presents a novel semi-quantitative method of the analysis of fluorescence microscopy images developed to provide a principled method of FRET detection. A model predicting the shapes of the spectra emitted by an arbitrary mixture of fluorophores, and subsequently of their multispectral images, provides a cross-reference between image colours and the levels of the individual fluorophores present in the mixture. The model is representative of all the relative combinations of the fluorophores. Once the model is constructed, for each pixel in a multispectral image the parameters corresponding to relative levels of the individual fluorophores are computed from the model. The distribution and the levels for each fluorophore is represented in the form of images, referred to as “parametric maps”.

The next section describes FRET in more detail. Section III outlines the modelling of the fluorescence emissions and of the imaging pathway, and sketches out the error analysis. The selection of the optimal filters and the implementation of the inversion process which computes the relative levels of the emission by a given fluorophore are presented in section IV. The remaining sections describe the experiments, their results and the conclusions.

II. FLUORESCENCE RESONANCE ENERGY TRANSFER (FRET)

Fluorescence is a phenomenon in which light at an appropriate wavelength excites electrons in a molecule; the electrons returning to a resting state emit energy at a longer wavelength. FRET involves two molecules (fluorophores). The donor molecule receives the initial energy from a photon whose wavelength is within a specific spectral excitation range. During the subsequent decay stage a photon with the longer wavelength is emitted. The acceptor molecule must have its absorption spectrum tuned to the emission spectrum of the donor molecule. When it receives a photon from the

donor it fluoresces (weakly) at a longer wavelength. The energy loss in a donor makes its own fluorescence level decrease. During FRET the energy transfer from the donor to the acceptor is radiationless. As FRET can only occur within 1-10 nm, the detection of the emission from the acceptor means that the two molecules are very close. If they are attached as markers to the proteins of interest, this is strongly indicative of the protein interaction. This evidence can be further corroborated by the drop in the fluorescence level by the donor molecule. FRET suffers from several problems of which the main ones are the low signal levels, the overlap of the donor and the acceptor spectra, the excitation of the acceptor by the donor excitation wavelengths, the cell autofluorescence and the background fluorescence.

The most commonly used method for the detection of FRET is co-localisation. More recently, a family of semi-quantitative methods have been developed, based on a simple model of interactions between the donor and the acceptor, under different illuminations [1-3]. The methods require the acquisition of up to 8 images which represent spectral responses of the fluorophores and the background fluorescence recorded through the filters matching the excitation and the emission spectra. The latest addition to the FRET detection methods is linear spectral unmixing (e.g. [4]), which requires the acquisition of the complete spectra. It assumes that a remitted spectrum is a linear combination of the constituent spectral emissions by the donor and the acceptor, with the background fluorescence normally subtracted.

III. PREDICTIVE MODELLING

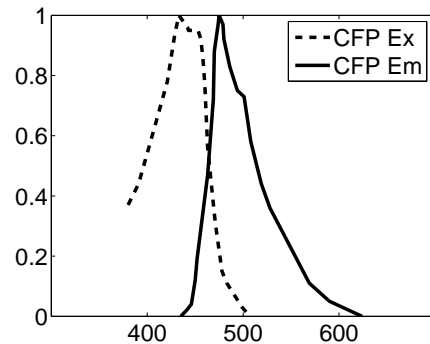
The analysis employed in this work draws on the understanding of the image formation process which can explain the relationship between the quantities we try to measure and the image values to which they correspond. Given the spectral definition of all the individual fluorophores that can be present in a sample it is possible to model the spectra resulting from their mixtures in different proportions (Sect. III.A). The subsequent modelling step computes the effects of transmission through spectral filters and the capture of photons by a camera sensors (Sect. III.B). In this way it is possible to predict image values originating from various mixtures of fluorophores. These predictions are then used to recover the parameter values from image values, as described in Section IV.

A. Fluorescence spectra

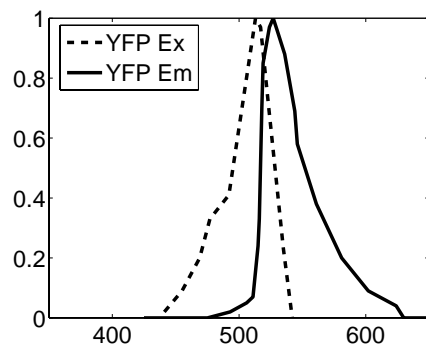
The pair of fluorophores used in this work is Cyan Fluorescent Protein (CFP) and Yellow Fluorescent Protein (YFP). Their respective excitation and emission spectra are shown in Fig.1(a) and (b). CFP acts as a donor in FRET and YFP as an acceptor. Fig.1(c) shows the CFP emission spectrum together with YFP excitation spectrum demonstrating the spectral overlap which is necessary for FRET (30% or more).

The spectra in Figure 1 are acquired by direct measurement

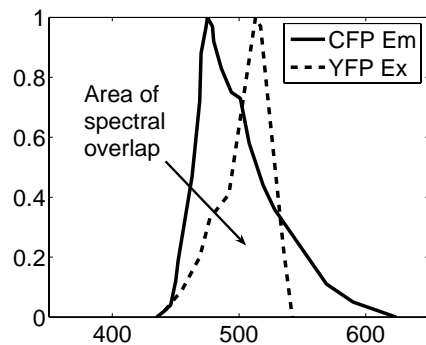
from pure fluorophore dyes [5] and normalized so that the peak emission has value 1. In practical imaging the magnitude of the emitted fluorescence depends on the magnitude of the excitation light (which “donates” photons), its spectral overlap with the excitation spectrum of the acceptor, and the local concentrations of the fluorophores. If a sample contains a mixture of CFP and YFP, its fluorescence spectrum should be a linear combination of their emission spectra, $PC(\lambda)$ and $PY(\lambda)$.



(a)



(b)



(c)

Fig. 1: Excitation (Ex) and emission (Em) spectra for (a) CFP and (b) YFP; (c) spectral overlap between the CFP (donor) emission range and the YFP (acceptor) excitation range necessary for FRET. The wavelength (nm) is shown along the x-axis, and the relative magnitude of spectral emissions as a function of wavelength is shown along y-axis.

A well known analysis method, known as spectral unmixing, uses this assumption of linearity to identify the contributions of individual fluorophores from spectra containing their mixtures [6]. However, the purity of these spectral responses is compromised by additional emissions which may originate from background fluorescence, cell autofluorescence and other sources. These unwanted background contributions (not noise!) are difficult to model theoretically, but they need to be incorporated into the model. In this case their theoretical modeling was replaced by the experimental collection of data from the slides containing cells not tagged with fluorophores. The principal component analysis (PCA) carried out on these spectra provided the mean spectrum, $PB(\lambda)$, and the first principal component and its range, quantified as b . The background spectra parametrised in this way were incorporated into the model and a full set of spectral emissions was generated by the equation

$$P(c,y,b,\lambda) = c \cdot PC(\lambda) + y \cdot PY(\lambda) + \mathcal{F}(b, PB(\lambda)) \quad (1)$$

where $c \in [0,1]$, $y \in [0,1]$, $b \in [0,1]$ (see III.C), and $\mathcal{F}(\cdot)$ is a non-linear function which predicts the combined background fluorescence and autofluorescence at level b given a statistical model of those emissions, $PB(\lambda)$.

Taken together this family of spectra constitutes a spectral emission model. The model has three variable parameters: the level of CFP emissions c , the level of YFP emissions y , and the combined auto- and background fluorescence b . Each combination of the quantities of c , y and b forms a parameter vector \mathbf{p} , which is associated through the model with the appropriate spectrum. Image values corresponding to the spectra are modeled by convolving each spectrum with the response functions of the appropriate colour primaries, for example red, green and blue. A vector of such primaries is called an image vector, \mathbf{i} . Section IV.B discusses in detail the selection of optimal filters for the recovery of the parameters.

B. Imaging system

In quantitative image interpretation it is necessary to take into account the optical properties of the imaging system. Their effect on the image can then be discounted so that pixel values can be directly related to the properties of interest. The optical properties are also needed for error analysis (see IV.A). In this work we have modelled the effects of a camera and of spectral filters. Camera quantum efficiency $Q(\lambda)$ specifies the percentage of photons registered at each wavelength λ . Filter transmission, $F_n(\lambda)$, specifies the percentage of photons transmitted through a given filter n at each wavelength λ . Normally the incident light spectrum has to be known, however in fluorescence imaging the light which stimulates the fluorophores is filtered out. The formation of an image vector $\mathbf{i} = [i_1, \dots, i_N]$ can be thus represented as

$$i_n = \int P(\lambda) \cdot F_n(\lambda) \cdot Q(\lambda) d\lambda, n=1, \dots, N \quad (2)$$

C. Multispectral emission model

Equation (1) in Section III.A describes how to model a spectrum originating from two known fluorophores $PC(\lambda)$, $PY(\lambda)$ and the background / autofluorescence emissions $PB(\lambda)$ present in a mixture at levels c , y and b respectively. The imaging system model described by equation (2) shows how to compute image values corresponding to a given emission spectrum $P(\lambda)$. By combining these two models together it is possible to predict image values (an image vector \mathbf{i}) corresponding to the parameter vector $\mathbf{p} = [c, y, b]$.

It can be assumed that in any given mixture the contributing emissions at any given point can vary between 0% and 100%. This provides (relative) constraints on the values of the parameters: $c \in [0,1]$, $y \in [0,1]$, $b \in [0,1]$. The 100% magnitude, or the parameter value of 1, corresponds to the situation where at a given image point the shape of the spectrum corresponds to the shape of a “pure” spectrum of one of the fluorophores (or the background / autofluorescence) as shown in Figure 1. On the basis of this assumption we can predict image values corresponding to an arbitrary mixture of fluorophores, or, in other words, an arbitrary parameter vector. For a given discretisation of the parameter ranges we can thus established explicit correspondence between *all* the parameter vectors and the image vectors:

for concentration c from 0 to 1 in steps of s_c
for concentration y from 0 to 1 in steps of s_y
for concentration b from 0 to 1 in steps of s_b
for filter n from 1 to N

$$i_n = \int P(c,y,b,\lambda) \cdot F_n(\lambda) \cdot Q(\lambda) d\lambda$$

A set of correspondences derived in this way forms a predictive model of image formation $f: \mathbf{p} \rightarrow \mathbf{i}$ which allows the computation of image values given the parameter values. However, our main interest is in the inverse procedure, i.e. the derivation of parameter values given the image values, $f^{-1}: \mathbf{i} \rightarrow \mathbf{p}$. This “model inversion” is possible if and only if there is a one-to-one correspondence between the parameter vectors and the image vectors over the entire range of the parameter values [7]. This condition can be tested by computing the Jacobi matrix

$$J_{mn} = \frac{\partial i_m}{\partial p_n} \quad (3)$$

for each \mathbf{p} and examining the sign of its determinant $J = \det(\mathbf{J})$. From the inverse function theorem [8], f is one-to-one and onto if and only if $J \neq 0 \forall \mathbf{p}$. If this condition is fulfilled,

there is a two-way correspondence between the parameter vectors and the image vectors, $\mathbf{i} \leftrightarrow \mathbf{p}$, which we refer to as the *multispectral emission model*.

IV. OPTIMAL FILTER SELECTION AND PARAMETER RECOVERY

The filter sets used in fluorescence imaging normally coincide with the emission peaks of the fluorescent dyes used. Our previous work [9] has shown that in quantitative analysis of spectral mixtures the best set of filters can be chosen through optimisation. The method for optimal filter selection is outlined in section IV.B. Prior to that section IV.A looks at error analysis because the error with which the contributions of the individual fluorophores can be recovered is used as an optimisation criterion in the filter selection process.

A. Error analysis

We have considered two sources of error. Spectral error is a statistical error arising from uncertainty in the measurement of spectra. Such measurements incorporate photon counting, which is known to be characterised by Poisson noise [10]. In this noise model the error is related to the photon count, $P(\lambda)$

$$\sigma_{spec}(\lambda) = \sqrt{P(\lambda)}. \quad (4)$$

The error for the image value i_n is thus [11]

$$\sigma_{spec}(i_n) = \sqrt{\sum_{\lambda} (\sigma_{spec}(\lambda) \cdot F_n(\lambda) \cdot Q(\lambda))^2}. \quad (5)$$

The camera error is the denominator in the expression for the camera signal to noise ratio (SNR) [12]

$$\text{SNR}_n(\lambda) = \frac{F_n(\lambda) \cdot P(\lambda) \cdot Q(\lambda) \cdot t}{\sqrt{F_n(\lambda) \cdot P(\lambda) \cdot Q(\lambda) \cdot t + D \cdot t + Nr^2}} \quad (6)$$

thus

$$\sigma_{cam}(i_n) = \sum_{\lambda} \sqrt{F_n(\lambda) \cdot P(\lambda) \cdot Q(\lambda) \cdot t + D \cdot t + Nr^2} \quad (7)$$

where $P(\lambda)$ is a photon count, $F_n(\lambda)$ - filter transmittance for filter n , $Q(\lambda)$ - quantum efficiency, D - camera dark current, Nr - the maximum readout noise and t is exposure time.

B. Optimal filter selection

The error analysis above supplies objective criteria for choosing the regions in the spectra where error is at its lowest. However, the aim of this work is to recover the magnitudes of the fluorescent emissions, i.e. parameters c , y and b forming vector \mathbf{p} . The optimisation criteria should be expressed in relation to these magnitudes. Using standard error propagation [11], the spectral and camera errors expressed as a function of parameter p_j are:

$$\sigma_{spec}(p_j) = \left(\sum_n (\sigma_{spec}(i_j) \frac{\partial p_j}{\partial \hat{a}_n})^2 \right)^{1/2} \quad (8)$$

and

$$\sigma_{cam}(p_j) = \left(\sum_n (\sigma_{cam}(i_j) \frac{\partial p_j}{\partial \hat{a}_n})^2 \right)^{1/2} \quad (9)$$

The total error is the sum of the total spectral error

$$\sum_j \sigma_{spec}(p_j) \quad (10)$$

and the total camera error

$$\sum_j \sigma_{cam}(p_j). \quad (11)$$

In the filter optimisation process filters are assumed to have Gaussian shape, normalised so that the area under the filter is 1. Each filter is defined by two values: the central wavelength (CW) and a full width at half maximum (FWHM). As for the recovery of three parameters (c , y and b) three filters are required, optimisation operates on a six-dimensional vector $[F_{CW1} \ F_{FWHM1} \ F_{CW2} \ F_{FWHM2} \ F_{CW3} \ F_{FWHM3}]$. A standard Matlab genetic algorithm GA [13] was used to find the optimal filter values. The outline of the algorithm is given in the Appendix. The use of GA as the means of optimisation is not crucial to this work; any optimization algorithm could have been used with an equal effect. Genetic algorithms belong to a class of stochastic optimization methods that normally suffer less from becoming trapped in local optima. In addition, the optimization criteria are very easy to specify as they do not depend on the specific structure of a problem. As the main focus of this paper is to present a methodology for determining an appropriate optimization criteria, a comparison of different optimization techniques is not included. Full details of the method for optimal filter selection can be found in [9].

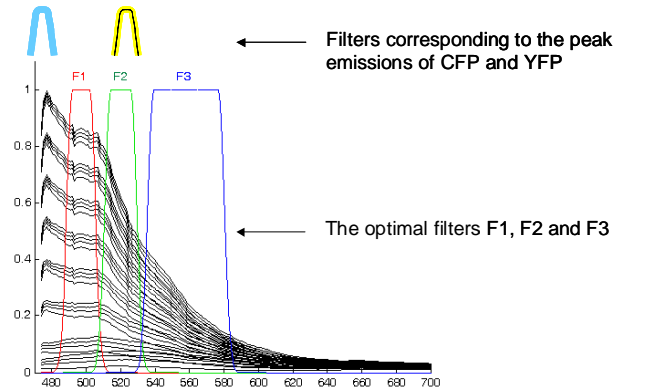


Fig. 2: The family of thin black lines shows a subset of the spectral emission curves generated by the forward model by varying parameters c , y and b . F1, F2 and F3 show graphically the locations and the extents of the imaging filters chosen by the optimization procedure and given numerically in section V. Two shapes shown above the graph show the locations of the filters coinciding with the peak emissions of CFP and YFP.

Figure 2 shows a subset of the spectral emission curves generated by the forward model (see Sec. III.A) with the superimposed filters selected by the optimisation algorithm. It is interesting to observe that the selected optimal filters do not coincide with the peaks of the emission spectra of CFP and YFP (see Fig. 2). One reason for this is that the choice of the filters is strongly influenced by the imaging system errors. The second reason is that in the spectral mixtures in which the spectra of the individual components overlap, the emission peaks are not necessarily the best locations at which to collect the spectra. The paper by Neher & Neher [14] comes to a similar conclusion.

C. Parameter recovery

The multispectral emission model developed in III.C comprises spectra which correspond to all the plausible combinations of parameters c , y and b . Now that the optimal filters are found, each spectrum can be substituted by a three-dimensional image vector \mathbf{i} where $i_{n,cyb}$ is a spectrum $P(c,y,b,\lambda)$ convolved with filter $F_n(\lambda)$.

The optimization procedure described in IV.B. has ensured that the mapping between the image vectors and the parameter vectors is one-to-one [9]. It is therefore possible to find a unique parameter vector $\mathbf{p} = [c \ y \ b]$ corresponding to a given image vector \mathbf{i} . If f denotes a function which maps the parameter vectors onto the corresponding image vectors, f^{-1} performs the inversion. In practice f^{-1} is non-linear and discrete, and its implementation has to involve interpolation to compute vectors \mathbf{p} for an arbitrary vectors \mathbf{i} . We have used an inversion algorithm based on the Taylor expansion [9]. The parametric image j is created simply by placing a value of a parameter p_j at a location (x,y) corresponding to $f^{-1}(i(x,y))$.

The accuracy of the parameter recovery has been tested on simulated data. A set of random parameter vectors $\{\mathbf{p}\}$ was generated and the corresponding spectra were computed using the forward model (see Sec. III). The spectra were contaminated with random noise (up to 5%) and digitally filtered by convolving them with the optimal Gaussian filters (see Sec. IV) to produce a set of image vectors $\{\mathbf{i}\}$ corresponding to the known parameter vectors $\{\mathbf{p}\}$. The image vectors were then supplied to the parameter recovery algorithm to compute a set of “recovered” parameters $\{\mathbf{p}'\}$. The original set \mathbf{p} and the recovered set \mathbf{p}' were then compared. Figure 3 shows graphically the comparison between the original and the recovered parameters.

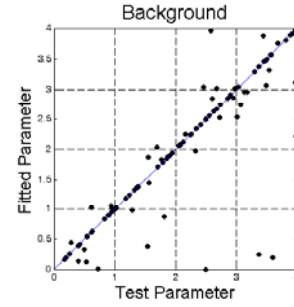
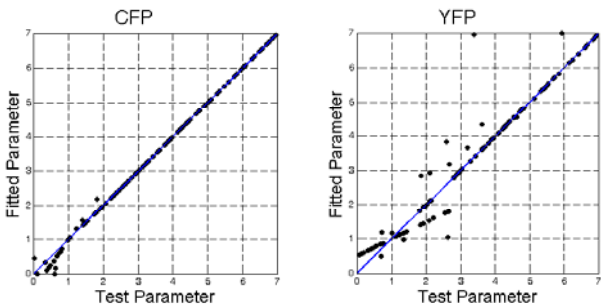


Fig. 3: Parameter recovery from the simulated data. The magnitudes of the randomly generated parameters are shown along the X-axis (Test Parameter); the parameters recovered through the model inversion are indexed along the Y-axis (Fitted Parameter). A thin diagonal line shows the locations where recovery is perfect.

V. EXPERIMENTS

The purpose of the experiments was to determine whether the new method correctly identifies fluorescence emissions from individual fluorophores (CFP and YFP), and correctly identifies the occurrence of FRET. The latter will be identified by the emission characteristic of YFP whilst illuminated with the excitation light in the wavelength range which excites CFP (but not directly YFP). As an additional sign of FRET, the YFP emissions will be at a lower level than in the presence of the YFP alone.

Phospholipase D1b (PLD1b) and ADP-ribosylation factor 6 (ARF6) are two proteins that have been shown to interact within cells by other methods and were therefore labelled with CFP and YFP respectively to facilitate the identification of FRET by this method (Powner et al., 2002). Four sets of sample slides were prepared: (a) a set containing untagged cells; (b) cells with CFP-labelled ARF6 protein only; (c) cells with YFP-labelled PLD1b protein only; and (d) a set where both proteins were labelled and thus likely to generate FRET. The slides were placed at a stage of the inverted fluorescence microscope (TE300, NIKON). White light generated by a mercury lamp was passed through a filter set BV-2A (400-440, CW=420) to produce illumination in the excitation range. A computer-controllable set of interference filters (VariFilters, CRI) was mounted between the microscope’s camera port and a high quality B/W digital camera (Retiga Exi, QImaging). Images were taken at the spectral wavelengths corresponding to the optimal filter bands $[F_{CW_i} \ F_{FWHM_i}] = [[497, 7]; [528, 8]; [558, 21]]$. The exposure time at each band was set individually to ensure as large as possible dynamic range and to avoid over- and under-exposure. Digital images were then numerically normalised to correspond to the same exposure time of 1 second. The inversion process was applied at every pixel and produced three parametric maps corresponding to the levels of CFP, YFP and the background.

VI. RESULTS

Figure 3 shows examples of the parametric maps for the four sets of experimental data. The image values have been

normalised to the maximum concentration (of each of the c , y and b) found in all the maps.

It can be seen that all the maps are qualitatively correct. Most excitingly, the last sample, in which FRET occurs, shows both the presence of YFP fluorescence and the drop in the level of CFP fluorescence. This is consistent with earlier findings (by another method) that PLD1b and ARF6 interact (Powner et al., 2002).

Some cross-talk can be observed between the maps of YFP and the background maps. This is partially an artifact due to the normalization used which can be corrected in the future versions of the software. However, as the plots in Figure 3 show, the error associated with the recovery of the background information is the largest of the three. Future work is needed to develop a better inversion procedure.

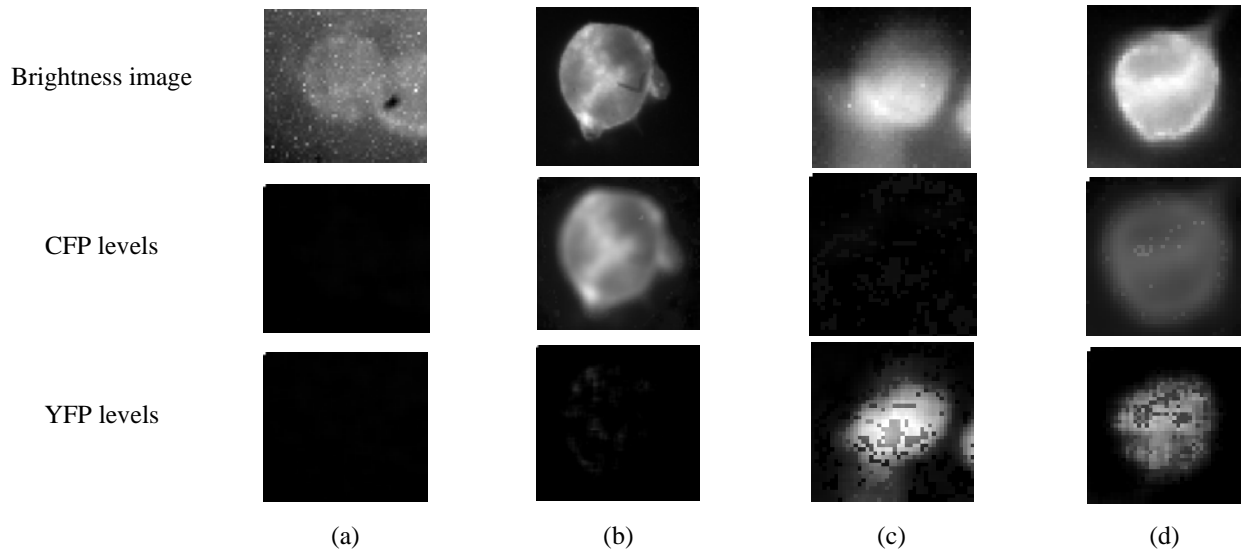


Fig. 4: (a) a set containing untagged cells; (b) cells with CFP-labelled protein ARF6 only; (c) cells with YFP-labelled PLD1b protein only; and (d) a set showing the evidence of FRET.

VII. DISCUSSION AND CONCLUSIONS

This paper has presented a new method of analysis of fluorescence images containing a mixture of fluorophores. It generates parametric maps, each showing a relative quantity of one individual fluorophore at a given location. Unlike spectral unmixing methods, this method does not require the acquisition of the complete spectral data. Instead, only several bandpass filtered images are needed, their number being equal to the number of fluorophores in the mixture plus one (to account for background fluorescence). The quantities in the parametric maps are related to the magnitudes of the fluorescence in the sample through a predictive spectral model. The method has been successfully applied to the detection of FRET, which provided evidence of interaction between proteins ARF6 and PLD1b in a cell. The work described in this paper constitutes “proof of concept” for the new method and space constraints have prevented inclusion of further detail. Additional systematic studies are planned to improve the model and to enable a full statistical verification. In particular, additional factors must be included in error analysis such as statistical errors associated with the “pure” emission spectra of the individual fluorophores, numerical

errors of the model inversion etc. The key reason for the cross-talk between the parameters presented in the parametric maps is a sub-optimal image acquisition system, and in particular the specification of the excitation filter. We have used an off-the-shelf filter cube whose parameters are not best suited for the particular combination of fluorophores.

In conclusion, we believe that the preliminary work described in this paper has provided a convincing evidence of the feasibility of our semi-quantitative approach and of its future potential in the studies of protein-protein interactions via FRET analysis.

ACKNOWLEDGMENT

The authors thank the Wellcome Trust UK for funding of this study. Advantage West Midlands has provided funding for the multispectral imaging equipment used in this work.

REFERENCES

- [1] Youvan DC et al. (1997) Calibration of Fluorescence Resonance Energy Transfer in Microscopy using genetically engineered chelating beads. *Biotechnology* 3, 1-18.

- [2] Gordon et al. (1998) Quantitative Fluorescence Resonance Energy Transfer measurements using fluorescence microscopy. *Biophysical Journal* 74, 2702-2713.
- [3] Xia Z, Liu Y (2001) Reliable and global measurement of Fluorescence Resonance Energy Transfer using fluorescence microscopes. *Biophysical Journal* 81, 2395-2402.
- [4] Zimmermann T, Rietdorf J, Pepperkok R (2003) Spectral imaging and its application in live cell microscopy. *FEBS Letters* 546, 87-92.
- [5] <http://www.bdbiosciences.com/clontech/gfp/excitation.shtml>
- [6] Zimmermann T, Rietdorf J, Pepperkok R (2003) Spectral imaging and its applications in live cell microscopy. *FEBS Letters* 546, 87-92.
- [7] Claridge E, Preece SJ (2003) An inverse method for the recovery of tissue parameters from colour images. *Information Processing in Medical Imaging (IPMI)*, Taylor C and Noble JA (Eds.) LNCS 2732, 306-317. Springer.
- [8] Schutz BF (1980) *Geometrical Methods of Mathematical Physics*. Cambridge University Press.
- [9] Preece SJ, Claridge E (2004) Spectral filter optimisation for the recovery of parameters which describe human skin. *IEEE Pattern Analysis and Machine Intelligence*, 26(7), 913-922.
- [10] Young IT (1996) Quantitative microscopy. *IEEE Engineering in Medicine and Biology* (Jan/Feb), 59-66.
- [11] Kendall MG, Stuart A (1969) *The Advanced Theory of Statistics*. (3rd Ed.): Charles Griffin & Co.
- [12] <http://www.microscopyu.com/tutorials/java/digitalimaging/signalnoise>
- [13] http://www.mathtools.net/MATLAB/Genetic_algorithms/
- [14] Neher R, Neher E (2003) Optimising imaging parameters for the separation of multiple labels in a fluorescence image. *Journal of Microscopy* 213, 46-62.
- [15] Powner DJ, Hodgkin MN, Wakelam MJO (2002) Antigen-stimulated activation of Phospholipase D1b by Rac1, ARF6 and PKC α in RBL-2H3 cells. *Mol. Biol. Cell.* 13, 1252-1262.

APPENDIX

The algorithm for the optimal filter selection

```

Generate a model set of spectra for known parameter vectors pk[c,y,b]
Generate a random set of filter definition vectors Fn[cw1,hw1,cw2,hw2,cw3,hw3]

Until the max number of iterations reached
  for each filter vector Fn

    convolve the three filters Fn with all the spectra in the model set
    this yields a set of image vectors Ik[i1,i2,i3]

    if the correspondence between all pk[c,y,b] and Ik vectors is NOT one-to-one
      FITNESS = 0
    else
      compute the fitness for Fn:  FITNESS = 1/Total_error
    endif

    delete the half of the filter vectors with the lowest FITNESS value
    retain the other half
    generate a full complement of the filter vectors by crossover and mutation

  end for
end until
The filter vector with the largest FITNESS value defines the optimal filter set

```
